Slowing-down processes, energy deposition, sputtering and desorption in ion and electron interactions with solids

J. Schou
Risø National Laboratory, DK-4000 Roskilde, Denmark

Abstract
The slowing-down processes of ions and electrons in matter are reviewed with special emphasis on the stopping cross-section. The relationships between elastic (knock-on) sputtering and nuclear stopping as well as between electronic sputtering and electronic stopping are discussed.

1 Introduction

Many phenomena which take place during ion, electron, and photon bombardment of solids are closely connected. These phenomena include energy loss of charged particles in solids, energy deposition and ejection of secondary particles during bombardment by charged particles. While the term sputtering usually comprises particles ejected as a result of momentum transfer to target particles or electronic transitions, desorption usually refers to the removal of less than a monolayer by electronic transitions at the very surface.

Sputtering as mass removal from the cathode during a gas discharge was discovered around 1850 [1], but the process was not understood, since the concept of 'charged particles' was not yet established. The discovery of radioactivity led to a big step forward towards well-defined ion sources [2]. Rutherford's famous work on the structure of the atom immediately stimulated work on particle slowing down and a number of papers on energy loss based on classical theory appeared during the following years. After quantum mechanical treatments became available, estimates on light ion and electron energy loss in matter could also be performed, but refinements of the theoretical framework are still continuing [2–3]. Sputtering of neutrals by keV ions was largely explained in the years 1960–1970 [4], whereas electronic sputtering (of insulators) is still a partly unresolved issue for non-elemental solids. Both types of sputtering could be explained by a relationship to the relevant part of the stopping cross-section (to be explained below). Secondary electron emission induced by ions was discovered around 1900, but the theoretical treatments did not appear until 1950–1980 [5]. Precise measurements of the desorption rates were not possible until reliable ultra-high vacuum systems were available. The leading theories were made around 1960 by Menzel, Gomer, and Redhead [6].

2 Stopping force (d*E*/d*x*)

2.1 Ion slowing down

The key quantity in energy loss considerations is the stopping force d*E*/d*x* (which in the past was named stopping power). This can be considered as the force that the medium exerts on the penetrating particle:

$$\mathrm{d}E/\mathrm{d}x = NS(E)\ , \tag{1}$$

where N is the number density of atoms in the medium and $S(E)$ the stopping cross-section, in which the dependence on the kinetic energy E of the primary particle is explicitly written. The stopping cross-section is a density-independent quantity except for ultrarelativistic energies and has the

dimension [energy × area]. In fact, many tables do not distinguish between stopping force (power) with the dimension [energy/length] and stopping cross-section, e.g., Ref. [7].

The theoretical framework for a general treatment of energy loss to the nuclei as well as to the electrons, i.e., the electronic system, was comprehensively treated by Bohr [8] and Lindhard *et al*., [9] in a number of important papers.

The collisions between the primary ions and the atoms in a solid can be divided into collisions between the primary particle and the nuclei, and those between the primary and the electrons. The first collisions take place for small impact parameters and lead to a large-angle scattering process, whereas the latter ones lead to energy loss without any significant deflection of the primary particle. The stopping cross-section $S(E)$ can be split up into

$$S(E) = S_n(E) + S_e(E) \quad (2) \tag{2}$$

where S_n is the nuclear stopping cross-section and S_e the electronic stopping cross-section. The term 'nuclear' is misleading, since the primary ion interacts with the screened nuclei rather than the bare nuclei.

The two stopping cross-sections drawn from the tabulations in Ref. [10] are shown in Fig. 1. The four regimes cover the low-energy (I), intermediate (II), high-energy (III) and ultrarelativistic regime (IV) (not shown in Fig. 1). The nuclear stopping is dominant in regime (I), but decreases gradually to less than a factor of the order $M_p/m \sim 2000$ than the electronic stopping (M_p is the proton mass) in regime (II). In regime (III) the electronic cross-section decreases monotonously.

An important scaling parameter is Lindhard's reduced energy ε:

$$\varepsilon = \frac{32.53 M_2 E}{Z_1 Z_2 (M_1 + M_2)(Z_1^{2/3} + Z_2^{2/3})^{1/2}} \tag{3}$$

where E is the energy in keV and the masses M_1 and M_2 are in amu. Lindhard and coauthors [11] showed that the nuclear stopping for all target–beam combinations could be expressed as

$$N S_n(E) = \frac{\pi a_L^2 \gamma N}{(\varepsilon/E)} s_n(\varepsilon) \tag{4}$$

where

$$\gamma = 4M_1M_2/(M_1 + M_2)^2 \tag{5}$$

is determined by the maximum energy transfer γE from a particle of mass M_1 with an energy E to a particle at rest with mass M_2 and by Lindhard's screening parameter

$$a_L = 0.8853 a_B \left(Z_1^{2/3} + Z_2^{2/3}\right)^{-1/2}. \tag{6}$$

The absolute magnitude is determined partly by the factor (ε/E) in the denominator, which means that for heavy atoms on a heavy target the factor becomes small and, in turn, leads to a large nuclear stopping. Equation (5) also demonstrates that ε decreases with increasing atomic number (and mass) of the projectile. The maximum of the nuclear stopping, which for the classical Thomas–Fermi model occurred at $\varepsilon \cong 0.3$, is therefore shifted to higher energies for heavy projectiles.

The reduced nuclear stopping power is usually calculated from a representative potential, the so-called KrC potential, for which several refined approximations exist [12]. The nuclear stopping shown in Fig. 1 is computed on the basis of the potential given in Ref. [12], which also is the underlying basis for Ref. [10].

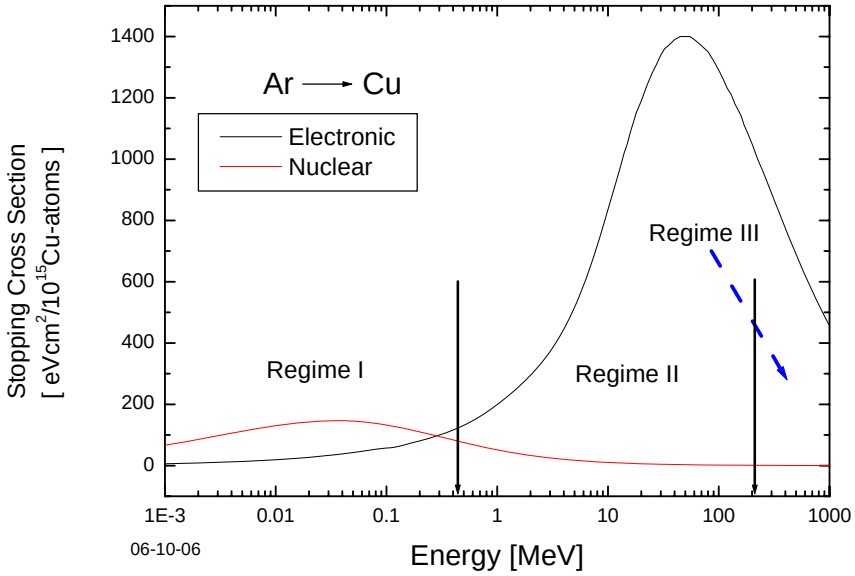

Fig. 1: Electronic and nuclear stopping cross-section for Ar ions incident on Cu. Data from Ref. [10].

The electronic stopping in the low-energy and intermediate regimes (I and II) can be determined by Lindhard–Scharff treatment [13]. The predictions from the Lindhard–Scharff model are usually correct within a factor of two, and can still be considered as a convenient reference standard. In reduced units the electronic stopping can be expressed as

$$S_e(\varepsilon) = k_L \varepsilon^{1/2} \tag{7}$$

where the constant of proportionality k_L depends on the atomic number and the mass of the beam atom and the target atom [9,13]. Except for very light ions on heavy targets, $k_L \cong 0.15$. The electronic stopping cross-section is thus proportional to the velocity and can be converted to real units with the same factor as the reduced nuclear stopping cross-section in Eq. (4). A number of treatments with improved accuracy have appeared [7,10,12,14], but the treatment of slow ions is still a difficult task [15].

With increasing velocity the projectile loses the electrons and at high velocities is completely stripped. At intermediate velocities in regime (II) the projectile electrons with velocities exceeding the projectile velocity v will stick to the projectile, while the slower ones, belonging to the outer shells, will be stripped. Sigmund [16] has estimated the broad maximum of the electronic stopping cross-section to be approximately at a velocity of $v_B Z_1^{2/3}$, where v_B is the Bohr velocity ($v_B \cong 2.188 \times 10^6$ m/s). For a proton ($Z_1 = 1$) this corresponds to a primary energy of 25 keV.

At high energies (regime III) the electronic stopping is determined by Bethe's or Bohr's treatment [2]. The decisive point is whether or not the problem can be treated by classical theory. This is possible for large values of Bohr's parameter [8]

$$k = \frac{2Z_1 e^2 v_B}{(h/2\pi)v} \tag{8}$$

where h is Planck's constant. In the quantum mechanical limit $k \ll 1$ Bethe's formula based on a first-order perturbation treatment gives the high-energy expression in the non-relativistic case valid for light ions:

$$S_e(E) = \frac{4\pi Z_1^2 Z_2 e^4}{m_e v^2} \ln \frac{2 m_e v^2}{I} \tag{9}$$

and $I \cong Z_2$ 10 eV is the mean ionization potential. For relativistic corrections the reader is referred to Ref. [2].

One notes that the condition for quantum treatment cannot be expected to hold for slow projectiles or projectiles of high atomic number. In this case the logarithm in Eq. (9) is replaced by Bohr's expression:

$$S_e(E) = \frac{4\pi Z_1^2 Z_2 e^4}{m_e v^2} \sum_{\nu=1}^{Z_2} \ln \frac{C m_e v^3}{Z_1 e^2 \omega_\nu} . \tag{10}$$

The major difference is that Z_1 enters into the argument of the logarithm, and therefore influences the position of the stopping maximum. Here ω_ν is a characteristic frequency of each electron level of the target atom, since the derivation is performed for a harmonic oscillator [2].

A complicating feature is the charge state of the incoming ions. According to Bohr's estimate [8], the average charge state of heavy ions is

$$Z_1^* = Z_1^{1/3} \frac{v}{v_B} \tag{11}$$

for the velocity range where $1 < Z_1^* < Z_1/2$. It means that the average ion charge state increases with the ion velocity. However, regardless of the initial ion charge state, which may be very far from the equilibrium charge state, an ion beam will approach charge state equilibrium after having penetrated a few layers from the surface.

There are deviations from the elemental stopping powers, in particular for slow ions. The gas–solid difference is largest for low-elements, but exceeds rarely a 10% correction. For chemical components the stopping force is close to the weighted sum of the components, but also here only minor deviations may appear [2].

The printed tabulations, Refs. [7] and [12], have been replaced by the popular code SRIM [10]. SRIM is based on an effective charge state which can be adjusted to experimental values but is not supported by a firmly established theoretical basis. Also Paul [14] and Paul and Schinner [17] have published extensive tabulations based on experimental stopping cross-sections.

2.2 Electron slowing down

In contrast to ion slowing down, electron slowing down has not undergone any substantial improvement since the 1980s except for development of electron codes for microscopy [18]. A number of computations have been incorporated in Fig. 2. For the simple case of a positron with kinetic energy E the Bethe treatment gives

$$S = \frac{4\pi e^4}{m_e v^2} Z_2 \ln \frac{m_e v^2}{I} . \tag{12}$$

For an electron, where one cannot distinguish between a scattered electron and a 'true' secondary one, the stopping cross-section becomes slightly modified:

$$S = \frac{4\pi e^4}{m_e v^2} Z_2 \ln \frac{a m_e v^2}{2I} , \tag{13}$$

where a = 1.1658 in the non-relativistic limit.

The stopping force up to 10 keV has been compiled by Schou in Fig. 2 [19]. The Bethe limit is seen clearly at high energies at which $S \sim Z_2/E$. However, at low energy the Bethe formula (13) is no longer valid, and the stopping is largely determined by density of free electrons in the material (for example, aluminium has the largest stopping because of the high density of free (conduction) electrons).

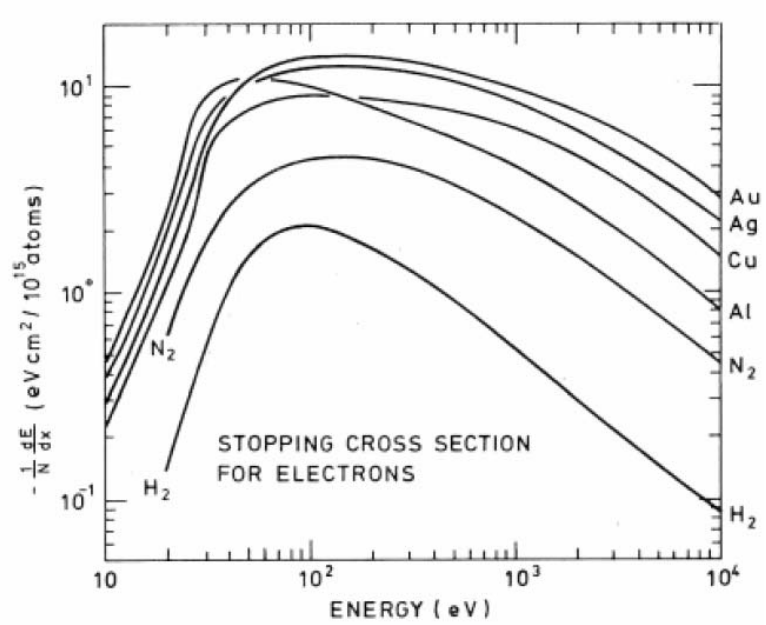

Fig. 2: Stopping cross-section for electrons in selected elements. From J. Schou [20]. (A part of the figure is published in Ref. [19].)

Range and stopping force calculations for electrons of energy higher than 10 keV have been performed by Berger *et al*. [21]. For energies above 10 keV, relativistic effects play a major role and the stopping cross-section falls off until about 1 MeV. Above 1 MeV the radiative component of the stopping force becomes dominant, and the total stopping increases strongly (Fig. 3). The energy loss by collisions is proportional to Z_2 and increases logarithmically with the energy, whereas the loss to radiation largely is proportional to Z_2^2 and increases practically linearly with the energy E [22].

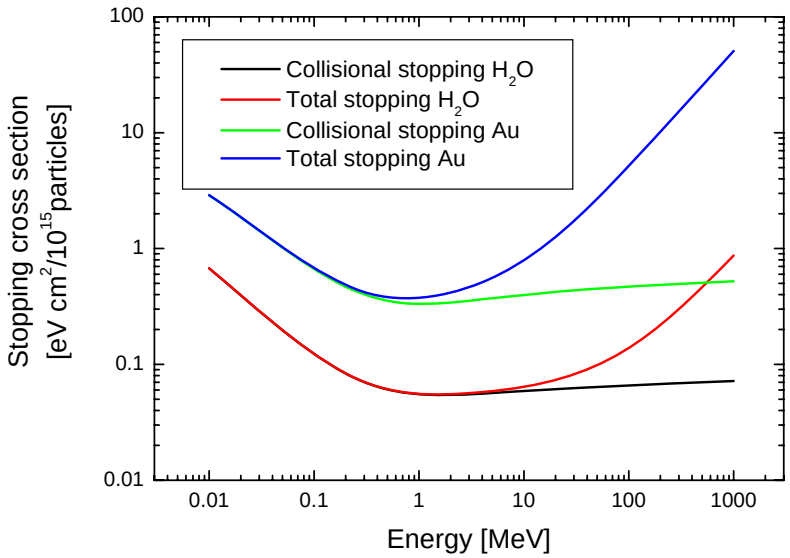

Fig. 3: Stopping of MeV electrons in liquid water and gold on the basis of the data in Ref. [21]

2.3 Energy deposition

The energy deposited by an ion is distributed in electronic excitations and kinetic energy that ends up in atomic motion and damage. Since the recoils may have a considerable range, the energy may be transported far away from the collision point. This means that the energy deposition can be substantially different from an energy-loss distribution. The theoretical work on the spatial distribution $F_D(E)$ of energy deposited in atomic collisions was initially performed by Winterbon *et al.* [23], and later published as extensive tabulations [24]. Distributions $D_e(E)$ for the electronically deposited energy by ions and their recoils were computed by Schou [25].

The energy deposited by electrons, e.g., in the keV range, is usually quite broad with a Gaussian profile, because of the pronounced scattering of the electrons. Deposition profiles have been published by Valkealahti *et al.*, [26]. Similar profiles for MeV electrons have been computed by Andreo [27].

3 Sputtering

3.1 Erosion processes

Material ejection from a solid can be induced by a number of processes which may even operate simultaneously (Fig. 4):

a) beam-induced evaporation,
b) collisional (elastic, knock-on) sputtering,
c) electronic sputtering, and
d) desorption of thin layers.

Sputtering is the erosion of material by single-particle impact in contrast to evaporation produced by many particles in beam-induced heating. Desorption is strictly speaking the removal of parts of a monolayer or full monolayers deposited on a different substrate. It is closely related to sputtering by electronic transitions, i.e., electronic sputtering. In the following only b) and c) will be treated. Beam-induced evaporation is treated by Schou in Ref. [28] and desorption in Ref. [6].

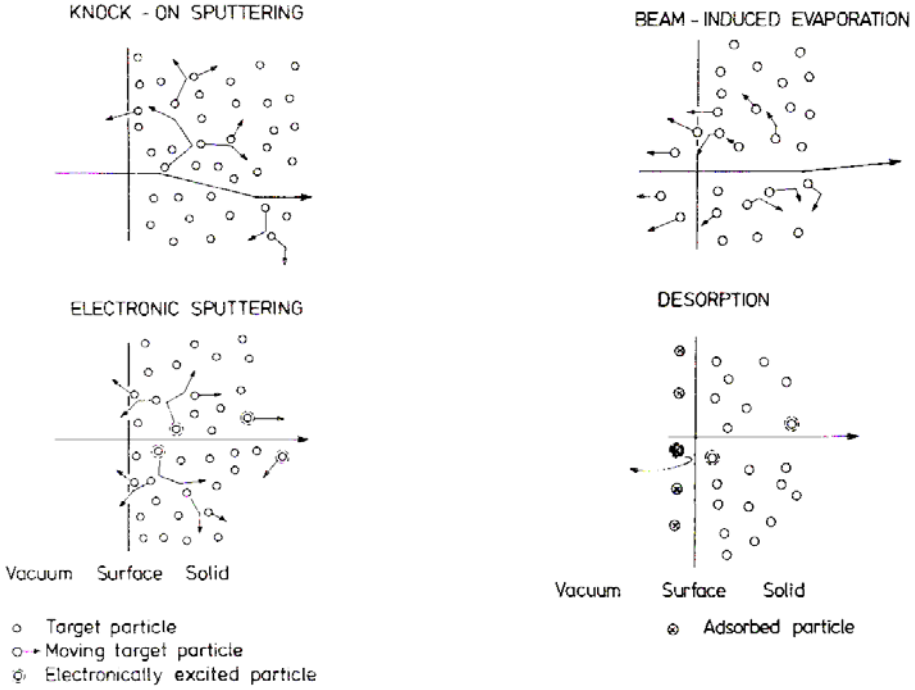

Fig. 4: A survey of different erosion processes. From Schou [29].

Reference [1] is still a classical reference for sputtering, while a more recent collection of papers on collisional and electronic sputtering can be found in Ref. [4].

The energy E deposited by a primary ion can be divided into the energy which is deposited into electronic excitations $\eta(E)$ and into atomic motion $\nu(E)$ according to Ref. [9]. These quantities can be expressed as the integral over the distributions $F_D(E,x)$ and $D_e(E,x)$:

$$E = \int F_D(E,x)\mathrm{d}x + \int D_e(E,x)\mathrm{d}x = \nu(E) + \eta(E) \ . \tag{14}$$

As mentioned above, the equation reflects the fact that the primary particle may generate recoils which undergo nuclear stopping as well, such that energy is transported away from the point of collision. It also means that the surface value $F_D(E,0) << NS_n(E)$ in many cases. In the case of very light projectiles the probability for backscattering increases strongly, and in this case $F_D(E,0) >> NS_n(E)$.

3.2 Collisional (elastic) sputtering

This type of sputtering is induced by the momentum transfer from the primary particle to the target atoms. Since the atoms are hit directly, the terms knock-on and ballistic sputtering have been used. A picture of the processes is shown in Fig. 4. The primary particle initiates a collision cascade via secondary or higher order collisions. Since the kinetic energy of the atoms set in motion is much larger than the binding energy of the material except for the last stage of the cascade, the standard treatment for metals can be largely extended to semiconductors and insulators.

The standard theory for sputtering is Sigmund's analytical theory [30] which is based on Boltzmann transport theory. The solution is obtained in the limit for high primary energy compared with the instantaneous energy of the cascade atoms. This corresponds to isotropic motion of the atoms in the solid. The treatment accounts for low collision densities in which the struck atoms in the cascade are at rest before the collision.

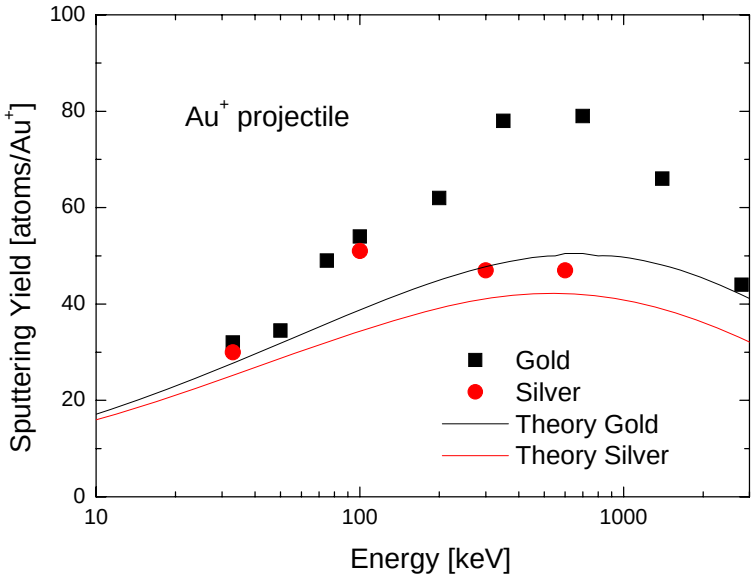

Fig. 5: Sputtering yield Y for Au ions on Au (black squares and line) and Ag (red circles and line). The solid lines are the predicted sputtering yield from Eq. (18). The deviations from theory occur in the so-called spike region, where the nuclear stopping is largest, in particular for the case Au+ ions on Au. Data from Bouneau *et al*. [31].

The (back)sputtering yield Y from a plane surface is given as

$$Y = \Lambda F_D(E,x) = 0 \ , \tag{15}$$

where $F_D(E,0)$ is the surface value of the spatial distribution of energy deposited into atomic motion. The constant Λ depends only on the material properties, the atomic density N, and the sublimation energy U_0 :

$$\Lambda = 3/(4\pi^2 N C_0 U_0) \, . \tag{16}$$

The cross-section C_0 ($\cong 1.81 \times 10^{-20}$ m^2) originates from a low-energy interatomic Born–Mayer potential and is common for all target materials in this approximation [1,30].

From dimensional arguments one may write

$$F_D(E, 0) = \alpha N S_n(E) \, , \tag{17}$$

where α is a function of the mass ratio M_2/M_1 (and of the angle θ of incidence which is not mentioned explicitly here). Here α is relatively insensitive for variations in the primary energy E, and can be well approximated by $\alpha \cong 0.17$ for most beam–atom target combinations, where $M_1 >> M_2$. This low value compared with unity also means that most of the energy deposited by the primary ion is transported away from the target surface by recoil atoms as discussed in the previous section. By combining Eqs. (16) and (17) one arrives at the well-known formula for the sputtering yield, in which no adjustable parameters enter [1,30]

$$Y = \Lambda \alpha N S_n(E) \, . \tag{18}$$

The linear-cascade theory has convincingly made it possible to predict important features of sputtering fairly well, and no other theoretical treatment has reached a comparable level [1,4,30]. Two beam atom–target atom combinations based on recent data are shown in Fig. 5.

An important exception from linear cascade theory occurs if the recoil cascades become too dense. This case, the spike regime, is characterized by a high collision density such that a moving atom in a cascade hits other atoms which have already been set in motion. The ‘spike’ yield is typically much larger than that from a linear collision cascade [1]. This is also seen in Fig. 5 for Au ions incident on the heaviest target material, gold, from 80 keV up to 2500 keV.

3.3 Electronic sputtering

Sputtering by electronic transitions, i.e., electronic sputtering, takes place primarily for insulating materials. A typical case is a volatile, frozen gas bombarded by light ions or electrons, but room-temperature insulators may also exhibit electronic sputtering [28,32]. The atomic motion is generated from repulsive potentials that arise during electronic de-excitation. The processes depend specifically on each material and can be extremely complicated for chemical compounds. The mechanism of electronic sputtering for the solid rare gases is now well understood, but the processes have not been fully identified even for a comparatively simple frozen material such as water ice [33].

In analogy to Eq. (16) the yield can be expressed by

$$Y = \Lambda (1/2) D_e(E, x = 0)(E_s/W) \, , \tag{19}$$

where $D_e(E, 0)$ is the surface value ($x = 0$) of the energy deposited into electronic transitions, E_s the energy produced by repulsive processes, typically a few eV, per ion generated by the primary ion, and W the energy required to produce an electron–ion pair (which is usually about 30 eV). Since the energy release from these non-radiative transitions is completely isotropic, one arrives at the factor (1/2) in Eq. (19). The equation is based on the assumption that the energy E_s is sufficiently large to generate a low-energy cascade. The factor (E_s/W) is usually much less than unity, since a considerable fraction of the energy is lost by luminescence from radiative transitions. Formula (19) cannot describe sputtering from a solid with mobile excitations, e.g., solid rare gases, but can give a qualitative trend for other frozen gases [28].

References

[1] *Sputtering by Particle Bombardment*, Ed. R. Behrisch (Springer, Berlin–Heidelberg, 1981).

[2] P. Sigmund, *Particle Penetration and Radiation Effects* (Springer, Berlin–Heidelberg, 2006).

[3] P. Sigmund, *Stopping of Heavy Ions* (Springer, Berlin–Heidelberg, 2004).

[4] *Fundamental Processes in Sputtering of Atoms and Molecules* (SPUT 92), Mat. Fys. Medd. Dan. Vid. Selsk. **43** (1993) 1, Ed. P. Sigmund.

[5] W. O. Hofer, in: *Fundamental Electron and Ion Beam Interactions with Solids for Microscopy, Microanalysis and Microlithography*, Eds. J. Schou, P. Kruit and D.E. Newbury (Scanning Microscopy International, AMF O'Hare – Chicago, 1990), p. 265.

[6] *Desorption Induced by Electronic Transitions, DIET1*, Eds. N. H. Tolk, M. M. Traum, J. C. Tully and T. E. Madey (Springer, Berlin–Heidelberg, 1983).

[7] H. H. Andersen and J. F. Ziegler, *Hydrogen Stopping Powers and Ranges in All Elements* (Pergamon, New York, 1977).

[8] N. Bohr, Mat. Fys. Medd. Dan. Vid. Selsk. **18**, no. 8 (1948).

[9] J. Lindhard, V. Nielsen, M. Scharff and P. V. Thomsen, Mat. Fys. Medd. Dan. Vid. Selsk. **33**, no. 10 (1963).

[10] J. F. Ziegler, SRIM (www.srim.org) 2006.

[11] J. Lindhard, V. Nielsen and M. Scharff, Mat. Fys. Medd. Dan. Vid. Selsk. **36**, no. 10 (1968).

[12] J. F. Ziegler, *Handbook of Stopping Cross Section for Energetic Ions in All Elements* (Pergamon, New York, 1980).

[13] J. Lindhard and M. Scharff, Phys. Rev. **124** (1961) 128.

[14] H. Paul, Stopping power graphs (www.exphys.uni-linz.ac.at/stopping) 2006.

[15] P. Sigmund, to be published.

[16] P. Sigmund, in: *Radiation Damage Processes in Materials*, Ed. C. H. S. Dupuy (Nordhoff, Leyden,1975), p. 3.

[17] H. Paul and A. Schinner, Atomic Data and Nuclear Data Tables, **85** (2003) 377.

[18] R. Gauvain, CASINO - (monte CArlo SImulation of electroNs in sOlids) (www.gel.usherb.ca/casino/) 2006.

[19] J. Schou, Scan. Micr. **2** (1988) 607.

[20] J. Schou, Thesis, Risø National Laboratory (1979) (unpublished).

[21] M. J. Berger, J. S. Coursey, M. A. Zucker and J. Chang (2005), *ESTAR, PSTAR, and ASTAR: Computer Programs for Calculating Stopping-Power and Range Tables for Electrons, Protons, and Helium Ions* (version 1.2.3). [Online] Available: http://physics.nist.gov/Star [2006, September 25]. National Institute of Standards and Technology, Gaithersburg, MD. Stopping-power and range tables for electrons, protons and helium ions (physics.nist.gov/PhysRefData/Star/Text/) 2006.

[22] H. A. Bethe and J. Ashkin, in: *Experimental Nuclear Physics*, Ed. E. Segré (Wiley, New York, 1953), pp.166–357.

[23] K. B. Winterbon, P. Sigmund and J. B. Sanders, Mat. Fys. Medd. Dan. Vid. Selsk. **37**, no. 14 (1970).

[24] K. B. Winterbon, *Ion Implantation Range and Energy Distributions,* Ed. D. K. Brice (Plenum, New York, 1975).

[25] J. Schou, Phys. Rev. B **22** (1980) 2141.

[26] S. Valkealahti, J. Schou and R. M. Nieminen, J. Appl. Phys. **65** (1989) 2258.

[27] P. Andreo, Nucl. Instrum. Methods, B **51** (1990) 107.

[28] J. Schou, Nucl. Instrum. Methods, B **27** (1987) 188.

[29] J. Schou, in: *Stucture-Property Relationships in Surface-Modified Ceramics*, Eds. C. J. McHargue, R. Kossowsky and W. O. Hofer (Kluwer, Dordrecht, 1989), p. 61.

[30] P. Sigmund, Phys. Rev. **184** (1969) 383 and **187** (1969) 768.

[31] S. Bouneau, A. Brunelle, J. Depauw, D. Jaquet, Y. Le. Beyec, M. Pautrat, M. Fallavier, J. C. Poizat and H. H. Andersen, Phys. Rev. B **65** (2002) 144106.

[32] R. E. Johnson and J. Schou, Mat. Fys. Medd. Dan. Vid. Selsk. **43** (1993) 403.

[33] R.A. Baragiola, R. A. Vidal, W. Svendsen, J. Schou, M. Shi, D. A. Bahr and C.L. Atteberrry, Nucl. Instrum. Methods, B **209** (2003) 294.